The Egyptian International Journal of Engineering Sciences and Technology

Vol. 30 (2020) 51–65

https://eijest.journals.ekb.eg/

ISSN:1687-1006

Artificial Neural Networks to Assess the Effect of Window Parameters on Indoor Natural Ventilation in "Sultan Al-Ashraf Qaytbay" Mosque

Amr Gomaa Mohammed *, Ahmed Farouk AbdelGawad , Mofreh Melad Nassief

Mechanical Power Engineering Dept., Faculty of Engineering, Zagazig University, Egypt

ARTICLE INFO

Keywords:

Archaeological mosque, Natural ventilation, Artificial neural networks, Wind tunnel experiments.

ABSTRACT

The Mosque of Sultan al-Ashraf Qaytbay is seen as one of the most beautiful features of late Egyptian Mamluk architecture. The architectural design of the mosque is exceptional due to its fine ranges and wonderful decoration. In this paper, Artificial Neural Networks (ANN) model was incorporated with wind tunnel experiments to investigate the properties of airflow within the Sultan al-Ashraf Mosque Qaytbay due to the natural ventilation caused by window openings. Wind tunnel experiments were utilized to supply the ANN model with the required data essential for the model training and establishment. The outcomes from the ANN model were validated using the results from the wind tunnel experiments. The comparison confirms the veracity of the ANN model results. Present results assured that it is very important to consider the aerodynamics and the bases of the natural ventilation when carrying out the restoration process by specialists to maintain the same performance of the original construction. ANN enables to easy predict the flow field when operating conditions are changed much easier and faster than the traditional computational and experimental methods.

1. Introduction

Ventilation is the air exchange between inside and outside conditions of a structure utilizing the wind flow which is viewed as a principal necessity to the building occupancy [1]. In moderate climates, common ventilation, in the present-day structures, is generally organized by open windows rather than specialized design elements. Appropriately, the position of window openings is viewed as a significant parameter deciding the adequacy of wind-driven cross-ventilation in buildings. Consequently, natural ventilation can spare the energy devoured by the heating, ventilating, and air-conditioning (HVAC) systems if it provides adequate indoor air quality and thermal comfort levels.

Sultan Al-Ashraf Qaytbay mosque, as appeared in Fig. 1, is an archaeological mosque that was constructed by Sultan Al-Ashraf Qaytbay in Cairo's Northern Cemetery, which is situated on Muizz Street. The Sultan Al-Ashraf started its construction in 826 AH/1424 AD and finished in 1474 AD [2-3]. The mosque is characterized by the excellence of its structural plan so that it was pictured on the Egyptian one-pound note.

* Corresponding author. Tel.: +201001079269
E-mail address: eng_amro_gh@hotmail.com

Figure. 1. A photographic view of Sultan Al-Ashraf Qaytbay mosque.

The mosque's entrance faces north and occupies the fundamental street somewhat eastwards around the walls of the tomb, perhaps to upgrade its special visualization. Figure 2 demonstrates a schematic outline of the Sultan Al-Ashraf Qaytbay mosque internal space.

The Qaytbay mosque is one of the oldest architectural monuments. The design of the mosque is complex, and exceptional as it is characterized by proportionality and the diversity of its motifs and inscriptions, inside and outside. The committee group consists of a mosque, a school, a dome, a sable, a book and seat for the Sultan, an animal watering basin, and a quarter of the residence. The area is estimated at 1088 m.

To the right of the door is the lighthouse, which rises to a height of 130 feet and consists of three turns and is one of Egypt's finest beacons. The entrance to the mosque heads north and turns the main road slightly eastward around the walls of the shrine.

The minaret is located above the entrance on the western side and is exquisitely carved from stone, divided into three floors with elaborately carved balconies. The eastern corner of the facade is occupied by Sable (through which water can be drained to bystanders) on the ground floor and by a letter (school) with open arches on the upper floor. The Qaytbay shrine projects from the east side of the building, which makes it more visible from the street and allows more light to reach the interior through the north facing windows.

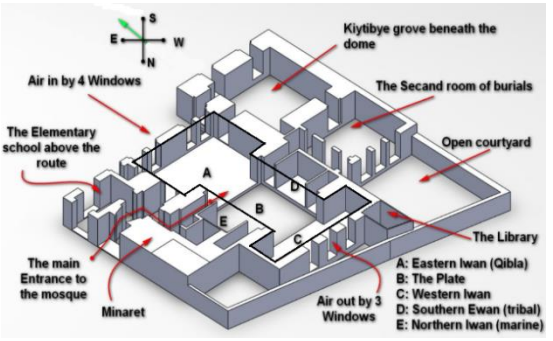

Figure. 2. Schematic diagram of the Sultan Al-Ashraf Qaytbay mosque internal space.

For concentration on natural ventilation, wind tunnel experiments are reliable tools for the determination of the impacts of wind loads on different structures in addition to the impact of natural ventilation on buildings, which is the particular purpose of this research.

In previous researches, wind flow with controlled speed moves over small models to recreate the regular ventilation of the structures. Wind tunnel investigations of natural ventilation were carried out by many researchers. Also, computation fluid dynamics (CFD) simulations were used for predictions of the details of natural ventilation that are difficult to address experimentally.

Wong and Heryanto [4] utilized computational fluid dynamics (CFD) simulations and wind tunnel experiments to study the capability of utilizing an active stack to upgrade regular ventilation in residential apartments in Singapore. Their outcomes identified the real-plan parameters that significantly impact the ventilation process. Also, wind tunnel experiments were carried out by Chu et al. [5] to examine the wind-driven ventilation for structures with two openings on a single wall. Their results demonstrated that the ventilation rate can be anticipated by the condition of the opening and that the conversion standard was relative to the root-mean-square of the pressure fluctuation. Wang et al. [6] exhibited an exploratory and numerical assessment of the effects of opening structures on ventilation rates. The predictions agreed with the measured results within an error of 25%. They stated that their models can be utilized for the structure of the ventilation systems.

Sacht et al. [7] provided the details of the results of wind-tunnel investigation for the assessment of the impact of the situating and sort of network of ventilation modules on a façade system. Their findings demonstrated that wind tunnel experiments

are a dependable methodology for the assurance of the impact of natural ventilation.

It was emphasized that the recent rampant propulsion of energy and material consumption at a brisk pace, which largely results from the staggering increase in population growth and economic development, has significantly threatened the very existence of our Earth [8]. The total energy consumption, approximately one-fifth of the energy worldwide goes to the construction sector, including commercial and residential units [9]. Therefore, the increased knowledge and interest of researchers in climatic changes have increased interest in energy consumption rates in buildings [10]. At the same time, and to achieve improved energy performance and reduced environmental impact, it was necessary to conduct studies for choosing the appropriate and healthy design to provide a great opportunity in saving energy and reducing environmental impacts [11].

In that context, a study in China [12] made a connection between the mechanical ventilation system in residential buildings and natural ventilation through the use of open windows. In five different climatic regions from north to south, the results showed that as the climate became warmer, the use of natural ventilation increased. According to the climatic conditions, the duration of natural ventilation was the longest in the summer and the shortest in the winter. The direction of using mechanical ventilation was the opposite of natural ventilation.

It was stated that, in general, by improving the structural design, the higher the temperature of the outside air, the less the energy consumption [12-13].

Also, Chena et al. [14] showed the importance of natural ventilation as a desirable feature for sustainable buildings due to its potential positive impact on building energy performance and amenities for its occupants. Natural ventilation can provide a higher rate of ventilation compared to mechanical ventilation, and this is through the use of natural ventilation in 12 American cities and has shown good results to reduce consumption energy.

Artificial intelligence has been used to measure the level of thermal comfort as it is a modern method of data analysis.

Artificial intelligence has been described as a computer form that coordinates human etiquette and exercises that require the use of intelligence [15]. An Artificial intelligence (AI) building modelling method can be used to predict the desired energy building outcomes, based on the associated variables, from environmental conditions and occupancy status [16]. Among the multiple methods that artificial intelligence used in research to predict outputs related to energy building, there was an advantage towards using artificial neural networks (ANN) compared to some other similar methods, including multiple linear regression (MLR), support vector machine (SVM) and decision trees (DT). The reason for this tendency is due to the myriad reported plus points embedded in ANNs adoption, such as good approximation capabilities, short development, and fast processing times [17]. Moreover, since training data using ANNs is not expensive compared to traditional data collection (such as theory-based or experimental methods), more and more researchers are interested in exploiting ANNs [18]. Therefore, it became necessary to use ANN, which is the best approach to study the rate of natural ventilation of residential areas to reduce energy consumption significantly with the connection to the primary goal of measuring thermal comfort and the rate of pollution to measure all effects.

Accordingly, Dai et al. [19] studied the rate of natural ventilation inside a residential building consisting of 24 floors, which was found to be insufficient at times. Therefore, it must be determined when the ventilation rate would be insufficient to create good quality indoor air with less energy consumption. Thus, they built an artificial neural network model (ANN) to predict the rate of ventilation at different times. They noticed that, on the last floor, the proportion of ventilation is less harmful than the first floor, which is a result of temperature variation and airspeed throughout the day, and it varies with different seasons. Furthermore, Afroza et al. [20] paid attention to the internal effects on energy consumption and thermal comfort in commercial buildings. Their study conducted an ANN model and entered all data to accurately predict the internal temperature to reduce energy consumption based on the results from the analysis of the obtained data. Park et al. [21] simulated the air in and around the building using an ANN model. They concluded that their proposed methodology allowed for the optimal windows designs corresponding to the variables for both individual and multiple activity models.

In light of the above overview of the past investigations, the following points illustrate a robust inducement to the present study and demonstrate its innovative significance:

1- Nowadays, most of the investigations consider modern buildings and structures. Although some of the modern mosques that were constructed in the twentieth century were

considered, little consideration was given to the natural ventilation of ancient mosques.

2- There is a narrow concern of the natural ventilation techniques that were applied in constructing the ancient mosques in Egypt, although the revision of ancient techniques of natural ventilation is an important subject in Egypt, considering the expected saving in energy and cost in comparison to the modern (artificial) ventilation techniques.

3- There is a growing interest in the application of developed ANN models due to their capabilities to improve building energy modelling and forecasting analysis. Majority of the studies incorporated ANN modelling focused on the prediction of the indoor air temperature.

4- In the present work, the natural ventilation is simulated utilizing an ANN model to demonstrate the influence of window openings on air velocity and pressure variation inside the mosque. Thus, the obtained ANN results are confirmed through the present experimental results obtained from the wind tunnel experiments.

5- Consequently, the present paper is a remarkable presentation of the utilization of ANN to the study of natural ventilation in historical buildings (e.g., mosques) in Egypt.

1. Experimental investigation

2.1 Wind tunnel

A wind-tunnel investigation was carried out with a reduced model of the investigated mosque to demonstrate the significance of the natural-ventilation characteristics of the mosque. The experiments were accomplished using a blowing open-circuit wind tunnel, Figure. 3. Details of the present experimental investigation are found in [22].

Figure. 3. Photo of the used wind tunnel.

A suitable blower (axial-fan) operates the wind tunnel. The total length of the wind tunnel is 6.0 m and situated 1.0 m over the floor. The test section is 0.6 m long with a square cross-section of 0.5 m × 0.5 m. As can be seen in Fig. 3, the tunnel is equipped with all necessary flow-conditioning setups to obtain uniform flow with the minimum boundary layer in the test section. The specifications of the driving motor of the blower (axial-fan) of the wind tunnel are listed in Table 1.

Table 1. Specifications of the axial-fan electric motor.

Specification	Value
Type	ADM-180M-4 NO
Power	15 *HP*
Speed	1480 *RPM*
Δ / Y	380 / 630
AMP	22.3 /12
Frequency	60 *HZ*

2.2 Experimental model

To replicate the airflow inside the mosque due to ventilation, a small-scale model was planned and constructed. Thus, the phenomena observed in both the model and the real mosque must be equivalent if the principles of physics and flow conditions are typically similar.

The present model signifies the main area of the mosque where the praying occurs. The overall dimensions of the mosque were obtained from the Egyptian Ministry of Antiquities [23] and through a field visit to the compound of Sultan Al-Ashraf Qaytbay. The scale-ratio of the model to the real mosque is 1:40. Therefore, the dimensions of the model are: length = 512 mm, width = 325 mm, and height = 400 mm. The model walls (faces) were fabricated from smooth acrylic plates of 4 mm-thickness, were precisely cut by a laser cutting machine. AutoCAD 2018 software was utilized to provide the necessary drawings for the laser cutting machine.

A number of 840 holes with a diameter of 1.7 mm were drilled in the model faces, which were used to insert the pressure taps that were made of small copper capillary tubes with a length of 10 mm and 1.7 mm diameter. The copper taps were fixed in place by a strong adhesive and connected to a multi-tube manometer by rubber tubes (hoses) of 2 mm diameter

for static-pressure measurements. CAD assembly drawing of the model is shown in Figure 4.

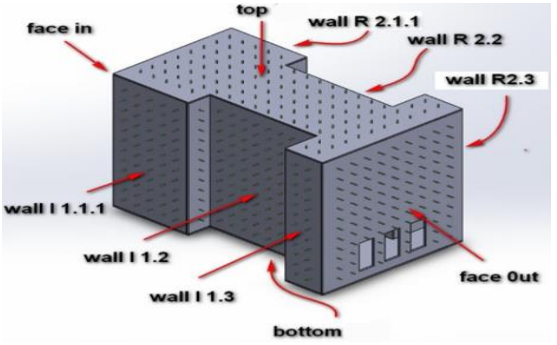

Figure 4. *CAD* assembly drawing of the model.

To eliminate the undesirable interference between the external wind flow and the copper taps, an external layer of walls was added to the model. Therefore, the external dimensions of the model are: length (l) = 580 mm, width (w) = 480 mm, and height (h) = 480 mm. Careful consideration was taken to prevent air leakage to the space between the internal and external walls of the model. Final assembly of the acrylic model is shown in Fig. 5. As it can be noticed in Figs. 5 and 6, the praying section has seven windows, four in the inlet face and three in the outlet face. The model dimensions of these windows are 35 mm-width (w) and 85 mm-height (h).

Figure 5. Photo of the model with the outer walls.

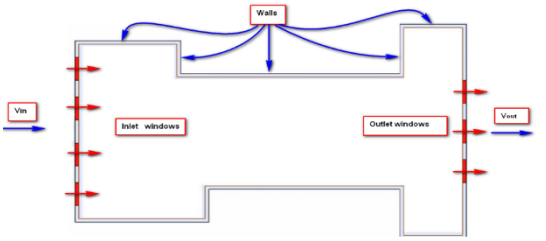

Figure 6. Layout of the praying section of the mosque model.

2.3 Experimental measurements

The measurements were concentrated on two main parameters, which are approaching the airspeed, and the static pressure (P) on the model walls.

A multi-tube manometer was used to measure the values of the static pressure. Because of the big number of measuring points in the present examination, a multi-tube manometer was built and used, Fig. 7a. As seen in Fig. 7b, the multi-tube manometer contained a metal holder of length 2.0 m, and height 1.5 m, and a wooden body of 1.5 × 1.5 m2. In the lower part of the wooden board, a 25 mm-diameter PVC pipe, drilled with 30 holes, was the feeder of the measuring liquid to the measuring glass tubes. One end of the feeder was closed while the opposite end was connected to a tank at a height of 50 cm above the feeder by a flexible hose. Thirty glass tubes with length1.0 m and diameter 8 mm were fixed at their lower end to the PVC feeder through the penetrated holes by an adhesive paste. The opposite ends of the glass tubes were connected to 30 flexible transparent hoses (tubes) with a diameter of 1.7 mm and length of 1 m. These flexible tubes were connected to the pressure taps on the model walls

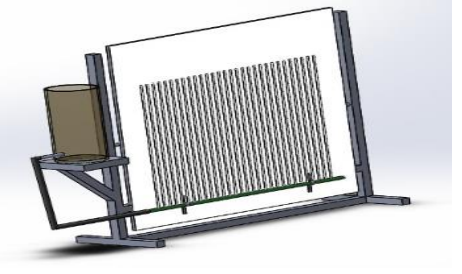

(a) *CAD* drawing.

(b) Photographic view.

Figure. 7. Multi-tube manometer of the present study.

Flow speed was measured by a standard Pitot-static tube, which was locally fabricated [24]. As shown in Figure 8a, the Pitot-tube was fabricated from a metal capillary tube (inner tube) of length 900 mm and diameter 1.7 mm capsulated in a steel tube (external tube). The steel tube comprised of two steel tubes of absolute length 550 mm, external diameter 8 mm, and an internal diameter of 5 mm. Likewise, two identical steel tubes of length 150 mm, external diameter 8 mm, and an internal diameter of 5 mm were connected to form straight T-and elbow-connections.

The lower parts of the two identical steel pipes were connected to the flexible transparent hoses that were connected to the two terminals of the U-tube manometer, Figure 8b. A nozzle of length 10 mm and external and internal diameters 8 mm, and 1.7 mm, respectively was fixed at the tip of the brass capillary tube (inner tube) to measure the total pressure. Three small openings of diameter 1.0 mm were bored on the steel tube (external tube). The three holes were equally distributed along the circumference of the tube to measure static pressure. At last, the Pitot-tube and its U-tube manometer were fixed on 200 mm × 300 mm steel board.

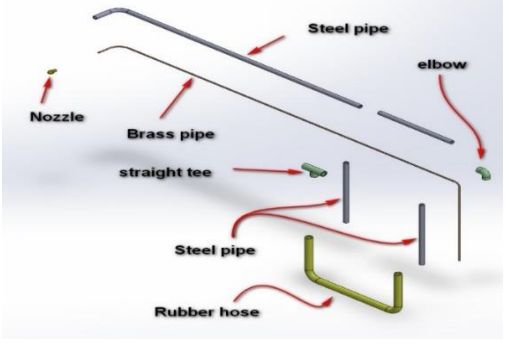

(a) Drawing of the components.

(b) Pitot-tube fixed in place during experiments.

Figure. 8. Pitot-tube of the present study.

To measure the velocity distribution of the approaching air flow towards the front face of the model by the Pitot-tube, the cross-sectional area of the wind tunnel, which is 480 mm × 480 mm with active zone 400 mm × 400 mm, was divided into rectangular/square grid cells. The border grid cells had dimensions of 50 mm × 25 mm, while the inner grid elements had dimensions of 50 mm × 50 mm. The measuring points were situated at the intersections of the grid cells. Consequently, the total number of measuring points was 64. The details of the frontal area with the grid cells are shown in Figure 9.

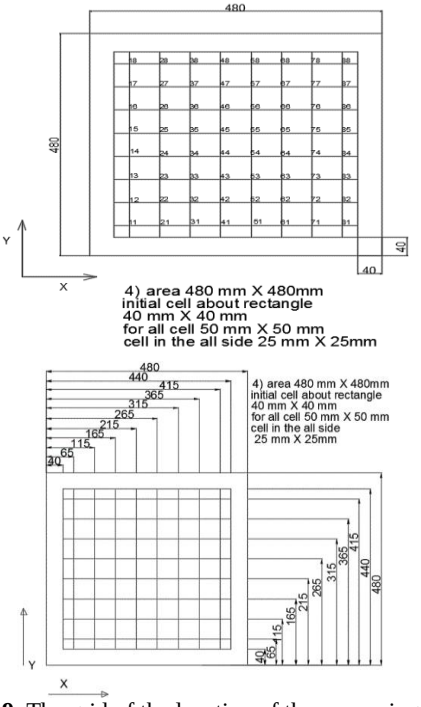

Figure 9. The grid of the location of the measuring points.

2.4. Estimation of Experimental Errors

The affectability of any device constrains its precision. The base division of an instrument implies

the minimum accurate readable value. Aggregation of the errors associated with estimating or ascertaining the parameters will cause the deviation of the determined results. The uncertainty in the calculated experimental results based on the uncertainties in the primary measurements can be estimated by the method presented by Kline and McClintock [25].

To assess the uncertainty in the determined results dependent on the uncertainties in primary measurements, the following formula is used:

$$\omega_R = \left[\left(\frac{\partial R}{\partial Z_1}\omega_1\right)^2 + \left(\frac{\partial R}{\partial Z_2}\omega_2\right)^2 + \cdots + \left(\frac{\partial R}{\partial Z_n}\omega_n\right)^2\right]^{0.5} \quad (1)$$

where, ω_R is the uncertainty in the final result, Z_1, Z_2, ..., Z_n are the independent variables, ω_1, ω_2, ..., ω_R are the uncertainty in independent results, R is the function of the independent variables Z_1, Z_2, Z_3..., Z_n. Then, the relative error λ_R (%) is defined as follows:

$$\lambda_R = \frac{\omega_R}{R} \times 100 \quad (2)$$

Thus, the relative error for each variable is calculated from the experimental data as follows; in pressure (P) ± 8.33%, in velocity (V) ± 0.21% and in the coefficient of pressure (Cp) ± 0.0047%

2.5 Pressure coefficient:

The pressure coefficient is a coefficient used in the study of compressible fluids and also non-compressible, where it describes the relative pressure in all flow releases of the fluid dynamics.

$$C_p = \frac{p - p_\infty}{\frac{1}{2}\,\boldsymbol{\rho}_\infty V_\infty^2} = \frac{p - p_\infty}{p_0 - p_\infty}$$

where:

p is the static pressure at the point at which pressure coefficient is being evaluated

p_∞ is the static pressure in the freestream

p_0 is the stagnation pressure in the freestream

$\boldsymbol{\rho}_\infty$ is the freestream fluid density

V∞ is the freestream velocity of the fluid, or the velocity of the body through the fluid

3. Present *ANN* Model

The human mind is a very complex system characterized by the ability to think, remember and solve problems. From this, there have become many challenges to compete with the functions of the brain and computer models. Although some great achievements are resulting from these efforts, all the models that have been developed so far are less when compared to the complex performance of the human brain [26].

Neurons are the basic units of cells in the system of the sensory mind. The artificial neuron cell is a similar component of the actual neuron, and as shown in Figure 10, the input signals are represented by X0, X1, ..., Xn. These signals are a group of continuous variables and are developed utilizing weight (sometimes called syntactic weight) and are either positive or negative equivalent to the increased acceleration of electrical flow signals [26].

In the present study, ANN was used to analyse airflow inside the "Sultan al-Ashraf Qaytbay Mosque" due to the natural ventilation caused by window openings to find the best way to create a suitable condition for worshipers in terms of thermal comfort. Therefore, a neural network was created and trained using datasets, which were collected from the experimental investigation (Sec. 2).

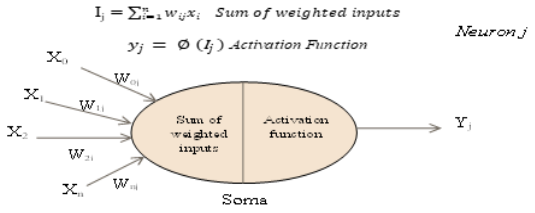

Figure 10. Schematic representation of an artificial neuron [26].

3.1 Definition of ANN

The artificial neural network has been defined as a system for processing data through simple and interconnected treatment elements (artificial neurons) in the structure of the cerebral cortex [27]. As shown in Figure 11, an ANN model usually has three layers: the input layer, hidden layer and output layer. It is a one-hidden-layer neural network with the rectified linear unit activation function [28].

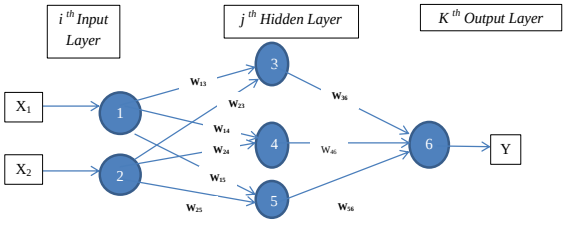

Figure 11. Simple *ANN* [26].

The output vector *Y* equals the raster output of the combined matrix and the input vector:

$$Y_k = W_{ij} \times W_{jk} \times X_j = W_{ij}k \times X_i \qquad (3)$$

Equation (3) shows that the relationship is linear. This indicates that three layers can be replaced with linear activation functions in the middle layer. This process introduced the concept of weight matrices, which is very useful in many situations [29].

3.2 Features of ANN

Four main highlights recognize the *ANN* models [26]

- They learn by model.
- They build up a circulated, acquainted memory.
- They are an adaptation to internal failure.
- They are fit for example acknowledgement.

3.3 ANN preparation and training

The ANN should be prepared in a few fundamental advances. The means are as per the following [26]

1. Apply irregular loads with little qualities (both positive and negative) to affirm that the system is not immersed by huge estimations of loads.
2. Select preparation work from the preparation set.
3. Insert the information vector to network input.
4. Calculate the yield from the system.
5. Calculate the blunder between the system yield and the ideal yield.
6. Adjustment of weight estimations of the system to limit this blunder.
7. Repeat stages 2-6 for each pair of information—yield vectors in the preparation set until the mistake for the whole framework is sensibly low.

In the present work, the preparation and training process was carried out based on the data collected from the present experimental investigation.

3.4 Design of ANN

An ANN is a computational model to design the neural network, the nervous system must be determined to correctly answer the problem and therefore requires a set of different parameters for the design of the neural network. These are the neural size, the choice of outputs, the function and type of activation, the layers, and the number of cells per layer [30].

In the present study, "MATLAB's Neural Network Toolbox (NNT) 2016a" was used to assemble the ANN, and through which, training, verification and testing the ANN design were carried out.

3.4.1 ANN layers

In this section, the developed ANN design, as a three-layer forward ANN as shown in Figure 12, is discussed.

The base layer is the input layer, which is made up of seven neurons four Input Variables (direction coordinates (X, Y, Z), Velocity Initial.) and three Output Variables (Cp, Vin, Tin) that are equal to the number of measured input parameters. Where, Vin, and Tin are the inlet velocity and temperature, respectively.

The input layer is connected to the hidden layer(s) containing several neurons. This number is an ANN design variable and is modified during the design process. The output layer contains three neurons, which represent the three output variables.

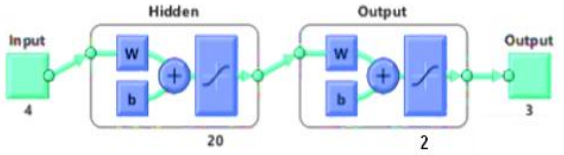

Figure 12. Present feedforward *ANN*.

3.4.2 Experimental data for ANN

Tables 2-4 show the study of advanced ANNs according to the design variables (hidden function - activation function - number of neurons). Grids are evaluated according to the graph of errors, training, testing, and general regression.

Thus, many cases were studied by changing the activation function as well as the number of neurons. Among them, a set of results was obtained to assess the best network to complete the study.

To simulate the experimental data, three different neurological states were chosen to determine the best results for the experiments, and thus the number of different neurons was determined as follows:

1- In the case of the activation function (Trainbr), the number of neurons changed from (10: 23).
2- In the case of the activation function (Trainlm), the number of neurons changed from (10: 20).
3- In the case of the activation function (TRAINLM and TRAINBR), the number of neurons was changed from (10: 22) and (10: 2), respectively.

Where "Trainbr" is Bayesian regularization backpropagation and "Trainlm" is Levenberg-Marquardt backpropagation [15].

Table 2. Neurons (Trainbr)

Net.name	No. Neurons	Activation Function	No. Hidden layer	Function Hidden
data1	10	Trainbr	1	Tansig
data2	11	Trainbr	1	Tansig
data3	12	Trainbr	1	Tansig
data4	13	Trainbr	1	Tansig
data5	14	Trainbr	1	Tansig
data6	15	Trainbr	1	Tansig
data7	16	Trainbr	1	Tansig
data8	17	Trainbr	1	Tansig
data9	18	Trainbr	1	Tansig
data10	19	Trainbr	1	Tansig
data11	20	Trainbr	1	Tansig
data 12	21	Trainbr	1	Tansig
data 13	22	Trainbr	1	Tansig

Table 3. Neurons (Tainlm)

Net.name	No. Neurons	Activation Function	No. Hidden layer	Function. Hidden
data1	10	Trainlm	1	Tansig
data2	11	Trainlm	1	Tansig
data3	12	Trainlm	1	Tansig
data4	13	Trainlm	1	Tansig
data5	14	Trainlm	1	Tansig
data6	15	Trainlm	1	Tansig
data7	16	Trainlm	1	Tansig
data8	17	Trainlm	1	Tansig
data9	18	Trainlm	1	Tansig
data10	19	Trainlm	1	Tansig
data11	20	Trainlm	1	Tansig

Table 4. Neurons (Trainlm and Trainer)

Net.name	No. Neurons	Activation Function	No. Hidden layer	Function. Hidden
data1	10 & 10	Trainlm & Trainbr	2	Tansig, Tansig
data2	8 & 12	Trainlm & Trainbr	2	Tansig, Tansig
data3	6 & 14	Trainlm & Trainbr	2	Tansig, Tansig
data4	4 & 16	Trainlm & Trainbr	2	Tansig, Tansig
data5	2 & 18	Trainlm & Trainbr	2	Tansig, Tansig
data6	2 & 20	Trainlm & Trainbr	2	Tansig, Tansig
data7	4 & 20	Trainlm & Trainbr	2	Tansig, Tansig
data8	2 & 22	Trainlm & Trainbr	2	Tansig, Tansig

3.4.3 Training data and transfer function

In this context, the implemented training algorithm is "spread the error again" [26, 15]. In the model of artificial neurons, this function is shown in equation (4) and its symbol and graph are shown in Figure 13. The above tables (2-4) illustrate the use of different data from Data name, Number of neurons, Activation function, Number of hidden layers, and Hidden function.

In this system, the calculation of the preparation carried out is "multiplication of back error". In a counterfeit neuron model, the amplitude of the exchange used is the x-capacity of hyperbolic prospecting (Tansig and Tansig).

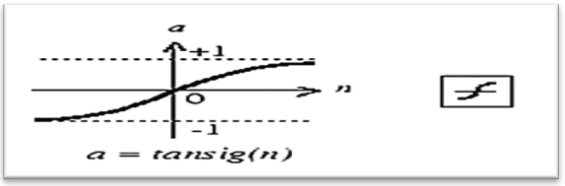

Figure 13. Transfer function symbol and graph of hyperbolic tangent sigmoid [15].

The hyperbolic tangent sigmoid function is expressed as

$$a(n) = \frac{2}{1+exp(-2n)} - 1 \qquad (4)$$

Hereafter, some examples of ANNs with different activation functions and many neurons are demonstrated. The developed ANNs were trained using the prepared experimental dataset, which consists of seven four Input Variables (direction coordinates (X, Y, Z), Velocity Initial.) and three Output Variables (Cp, Vin and Tin) normalized input parameters.

The training was conducted with a different number of neurons in the hidden layer. For training, 70% of the data set was used. For every training cycle, the difference between the ANN output and the desired output was calculated as the error of ANN output.

The training operation was continued until the error of the ANN output reached a preselected threshold value of mean-square-error (MSE) of 0.0001, Equation 5. If this value did not reach until epoch 1000, the training process stopped.

$$\boldsymbol{Mean\ Square\ Error\ (MSE)} = \frac{\sum(\pm \boldsymbol{error})^2}{\boldsymbol{n}} \qquad (5)$$

Another 15% of the data set is used for the validation of the developed ANN. The remaining 15% of the data set is used for the testing of the developed ANN. Finally, the error that proved present at the testing stage was identified. The training regression (R) is the correlation coefficient between the ANN output and the desired output. The maximum value of R is one. The high is the R the better is the correlation between the output and the desired output.

Figure 14 shows training results for NET-6 with 23 neurons in the hidden layer. The MSE threshold value was reached in stage 100. At this stage, the value of the training regression was 0.9026. To verify and test R is 0.91838 and 0.90414, respectively. For all samples, R is 0.90496.

Figure 15 shows the output error histogram of Net-6. It shows the distribution of the error values. The y-axis is the samples (instances) and the x-axis is the error (Target-Outputs). Most of the data are allocated in the middle of the histogram with 0.00293 errors, and a small number of the samples are allocated in the outer range with a higher error. The negative sign of error means that the output of the ANN was lower than the target.

Figure 16 shows the performance graph of NeT-6 training. The y-axis is the Mean Square Error (MSE) and the x-axis is the number of epochs. The best validation performance is 1.

4. Results and Discussion

In this section, experimental results and ANN are discussed. Where, the airspeed was set at 20 m/s, due to confinement in the experimental facility. Air velocity and pressure values are determined and tested on different walls of the model as well as flow lines and their examination.

4.1 ANN model results

Tables 5-7 show the analysis of the test set for each of the regression values (correlation coefficient) of the sophisticated networks. The regression value was used as a performance indicator. The regression value was the measure of the correlation between input and output. It had values from zero to one for the full link. Increasing or decreasing the number of neurons in the hidden layers affected the test regression, verification, training, training, and total values.

The work sequence was as follows:

1. Enter the dataset as an 840 × 7 arrays (840 dots, 7 input values)
2. Enter the *ANN* conversion function
3. The inclusion of activation functions (trainlm, trainbr)
4. Enter the number of neurons (as previously mentioned)
5. 70% of training input data sets, 15% for testing and 15% for certification.
6.. Repeat the sequence until an acceptable gradient value is reached.

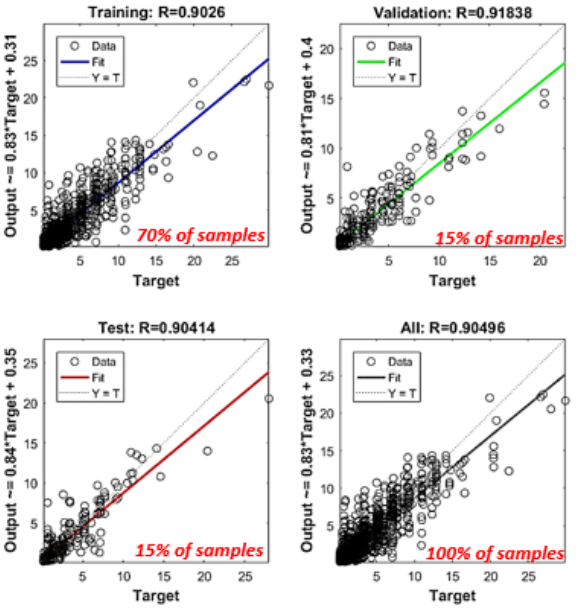

Figure 14. *ANN* outputs vs. target outputs during training, validation, and testing.

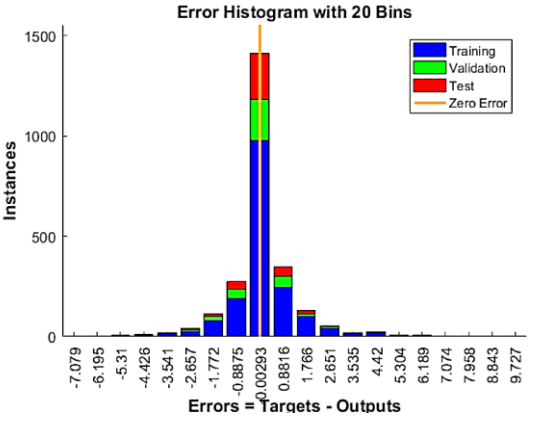

Figure 0. Error Histogram of Net-6.

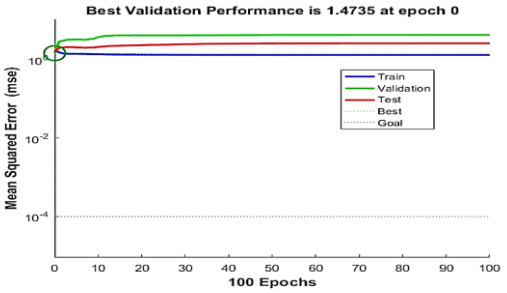

Figure 16. Performance graph of Net-6.

Table 5. Different Neural Networks (Activation Function – Trainlm & Trainbr)

Network code	Activation Function	No. Neurons	Function Hidden	Train regression	Validate regression	Test regression	Ovrall regression
Net-1	trainlm & trainbr	10 & 10	tansig, tansig	0.88048	0.89439	0.85687	0.87928
Net-2	trainlm & trainbr	8 & 12	tansig, tansig	0.86633	0.91608	0.91811	0.8832
Net-3	trainlm & trainbr	6 & 14	tansig, tansig	0.87372	0.91107	0.90421	0.88515
Net-4	trainlm & trainbr	4 & 16	tansig, tansig	0.9.336	0.85669	0.84644	0.88675
Net-5	trainlm & trainrb	2 & 18	tansig, tansig	0.87905	0.89866	0.8909	0.88231
Net-6	trainlm & trainrb	2 & 20	tansig, tansig	0.9026	0.91838	0.90414	0.90496
Net-7	trainlm & trainrb	4 & 20	tansig, tansig	0.85076	0.86389	0.81189	0.84624
Net-8	trainlm & trainrb	2 & 22	tansig, tansig	0.8596	0.88362	0.85842	0.86179

Table 6. Different Neural Networks (Activation Function – Trainlm)

Network code	Activation Function	No. Neurons	Function Hidden	Train regression	Validate regression	Test regression	Overall regression
Net-1	trainlm	10	tansig	0.87251	0.88233	0.83865	0.86926
Net-2	trainlm	11	tansig	0.87397	0.84072	0.86545	0.86754
Net-3	trainlm	12	tansig	0.83342	0.88261	0.88212	0.84946
Net-4	trainlm	13	tansig	0.87449	0.86465	0.8785	0.87319
Net-5	trainlm	14	tansig	0.90139	0.88201	0.85848	0.89222
Net-6	trainlm	15	tansig	0.87575	0.8708	0.83171	0.8679
Net-7	trainlm	16	tansig	0.87726	0.84181	0.80887	0.86362
Net-8	trainlm	17	tansig	0.89786	0.89218	0.91054	0.89909
Net-9	trainlm	18	tansig	0.88191	0.8882	0.87052	0.88106
Net-10	trainlm	19	tansig	0.87242	0.87801	0.8921	0.87637
Net-11	trainlm	20	tansig	0.61373	0.55462	0.71569	0.62505

Table 7. Different Neural Networks (Activation Function – Trainbr)

Network code	Activation Function	No. Neurons	Function Hidden	Train regression	Validate regression	Test regression	Overall regression
Net-1	trainbr	10	tansig	0.88048	0.89439	0.85687	0.87928
Net-2	trainbr	11	tansig	0.89263	0.85224	0.88302	0.88515
Net-3	trainbr	12	tansig	0.87448	0.91983	0.91258	0.8886
Net-4	trainbr	13	tansig	0.8872	0.87108	0.83539	0.87775
Net-5	trainbr	14	tansig	0.8921	0.87385	0.91832	0.89373
Net-6	trainbr	15	tansig	0.88863	0.87246	0.9088	0.88858
Net-7	trainbr	16	tansig	0.89048	0.90857	0.87374	0.89017
Net-8	trainbr	17	tansig	0.91427	0.89137	0.86848	0.90467
Net-9	trainbr	18	tansig	0.89209	0.88509	0.87576	0.88834
Net-10	trainbr	19	tansig	0.84454	0.83365	0.89096	0.84998
Net-11	trainbr	20	tansig	0.89721	0.921	0.90705	0.90236
Net-12	trainbr	21	tansig	0.90457	0.89233	0.90595	0.90299
Net-13	trainbr	22	tansig	0.88744	0.87038	0.84178	0.87651

For each ANN designed and tested, it is compared and analysed to determine the best result. The difference between them was due to a change in the number of neurons. This value indicates the ANN output dispersion level. From the above, it is clear that (NET-6), specified in the Tables 5-7, was the best investigator in all the data entered to ANN in terms of Train regression, Validate regression, Test regression, and Overall regression.

4.2 Comparison between ANN and wind tunnel measurements

Figure 17 demonstrates a comparison between the experimental and ANNs values of Cp at an airspeed of 20 m/s on various walls of the model. The values of Cp were averaged over the entire wall. The differences between the ANNs and experimental results may be attributed mainly to the fact that the number of measuring points on each face was limited. This is due to the limited space of the experimental model. Thus, the averaging of the ANN results on each face is expected to be more accurate than the averaging of the experimental results on the same face as the measuring points do not cover the whole surface. Furthermore, the effect of the measuring uncertainty, even its small magnitude, is expected to show up when compared with the ANN results.

It can be seen from these figures that the pressure increments at all edges of the model with a reduction occurring in the middle passage because of the reduction in the flow area. For both inlet and outlet walls, higher pressure values can be seen at the top segment contrasted with the lower partition because of the presence of window openings at this segment.

Likewise, it can be seen that at the window openings, the pressure decreases significantly which can be credited to the small zone of the window openings. Moreover, it is commendable to take note of the uniform pressure conveyance that is seen over the top wall (roof) of the model for both experimental and ANN results, which can be credited to the high elevation of the wall and the distance from the window openings.

Moreover, the convergence of results from the comparison shows that the greater the airflow, the greater the sense of thermal comfort and that the airflow in the middle area is better than the entire length of the model due to the movement of the air in a straight line without obstacle. In the movement of air, making it an unstable or turbulent area due to the difference in the size of the area. This disorder makes it an uncomfortable place, which means the middle area is better, as the air changes faster because there is

no obstacle preventing air from moving from the rest of the areas. When the movement of air on the walls and corners decreases, the hot air rises to the top, making the roof more disadvantageous in the good air.

face	ANN	Experimental
	V = 20 m/s	V = 20 m/s
	Cp	

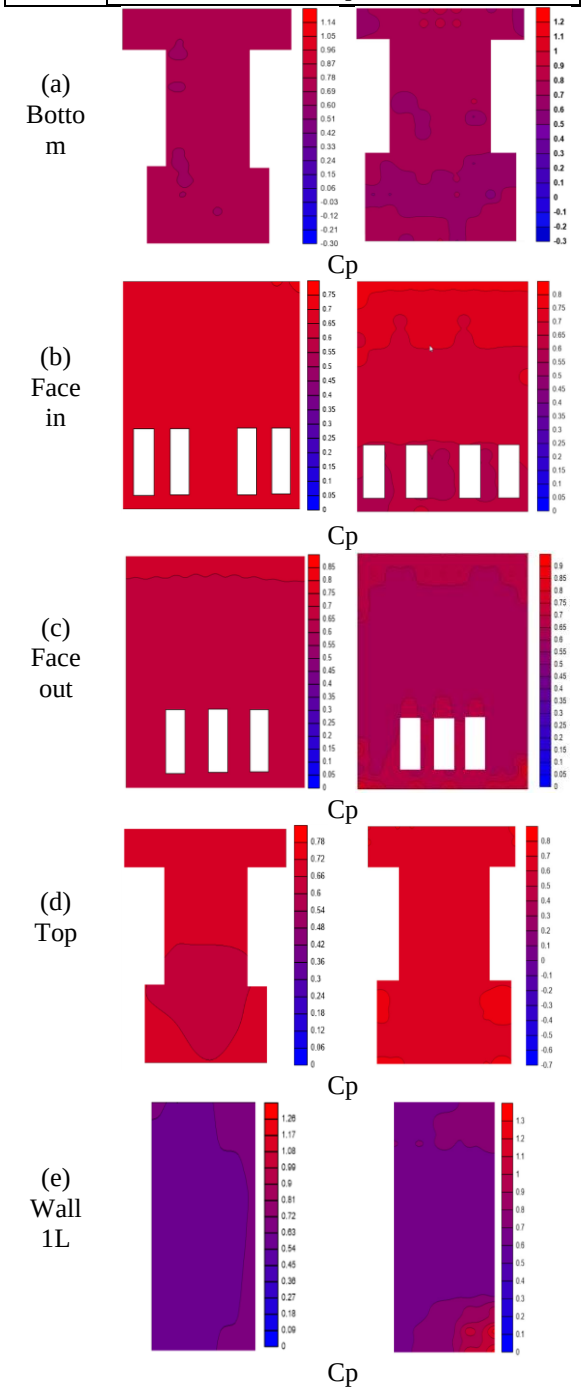

Figure. 17. ANNs and experimental results for the coefficient of pressure.

For more validation of the accuracy of the present ANN model, Figure 18 illustrates a comparison between the ANN and experimental results at a line above the ground by 0.8 m on the sidewall. Generally, the comparison of the results endorses confidence in the ANN results.
The maximum discrepancy is in the range of 0.5 - 1% of the relationship

$$Deviation = \frac{cp_{exp} - cp_{comp}}{cp_{comp}} x\ 100\% \quad (6)$$

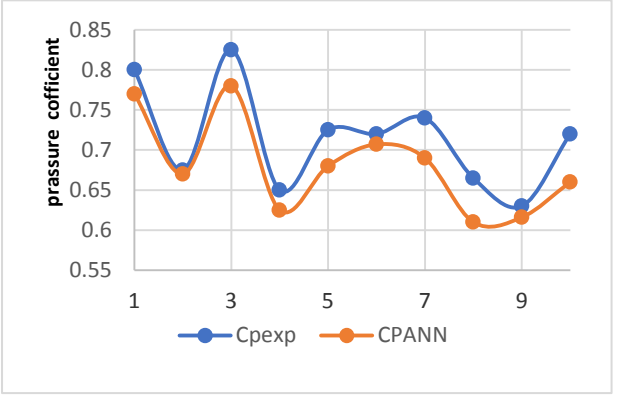

Figure. 18. Comparison between present experimental and ANNs values of Cp at 20 m/s.

In summary, the present study examined the natural ventilation of an old building in the historical area of Cairo, the Sultan al-Ashraf Mosque, Qaytbay, at a later time. The current study dealt with the natural ventilation of an old building in the historical area of Cairo, the Sultan al-Ashraf Mosque, Qaytbay. Based on the result and the above discussion of the current experimental and ANN model, the following closing points may be mentioned:

- From Figure 17b it can be shown that immediately after the interface (entry windows) of the model are the lowest places in terms of feeling thermal comfort in addition to the angles.
- As shown from Figures 17 g-h After the air passes through the window openings and after a distance of 1 meter, the air spreads over the entire area with a proportional distribution, which causes some improvement, and in the middle area the air differs better but the airspeed is lower and this appears on the walls in the form of e - f
- As for the Figures 17 (i - j), it is a weak ventilation area, as the air passes from a smaller area to a larger area, which makes the air turbulent due to its spread in the larger area.
- As for the Figure17c, the space in front of the exit windows is uncomfortable due to the exit of hot air, as the air is loaded with some pollutants from odours and others.

Conclusions

Based on the present study and the above results and discussions, the following points can be also enlisted:

- At present, due to the presence of buildings surrounding the mosque, a decrease in the amount and nature of the wind current within the mosque was observed, which led to a decrease in the flow of wind inside the mosque through the windows. As a result, thermal comfort is expected to decrease due to increased air temperature.
- The current research proposes to amend this ancient architectural design of the mosque to improve the airflow through the mosque and enhance the effectiveness of the mosque's ventilation under the current situation.
- The use of the *ANN* model method added a significant addition in light of accurate results, easy implementation, and accurate forecasts.
- The use of *ANN* model is dependent on data and information collected for use on the network. Data can also be modified during experiments to achieve the best results.
- *ANN* model can be improved over time by collecting new data to update information, data and variables to get the best results.
- It was found that the mosque, in its current status, needs some necessary adjustments to be better in terms of thermal comfort. Actually, the original design of the mosque had some more openings that added fresh air and helped in removing the warm and hot air. However, these openings are currently closed. Therefore, the inlet and exit upper windows, which are currently closed, must be reopened, which have the same dimensions of the currently open windows. This will allow a suitable volume of air to enter the mosque. Also, opening the exit windows increases the rate of exit of the polluted and hot air. Also, there are four air traps in the middle of the mosque, which are

currently completely closed. Originally, their function was either increasing the volume of inlet air in the center of the mosque or drawing out the hot air. In this way, the volume of air flow increases, which greatly helps in adjusting the level of thermal comfort inside the mosque. These four air traps should be reopened.

Nomenclature

Symbol	
AI	Artificial Intelligence
ANN	Artificial Neural Network
AH	Hijri calendar.
AD	Hijri calendar.
CAD	Computer-Aided Design
CFD	Computational Fluid Dynamics
Cp	Pressure Coefficient
DT	decision trees
HVAC	Heating, Ventilation and Air conditioning
h	Height, *mm*
L	Length, *m*
MSE	Mean-square-error
MLR	multiple linear regression
NNT	Neural Network Toolbox
P	Pressure, N/m^2
p_0	the stagnation pressure
p_∞	the static pressure
PVC	Polyvinyl Chloride
R	Final Result
SVM	support vector machine
T	Temperature
Tin	Inlet temperature
V	Velocity, *m/s*
Vin	Inlet velocity
V_∞	freestream velocity
W	Width, *m*
x, y, z	Three-dimensional coordinates
$X_0, X_1, ..., X_n$	Input signals
Y	Output signals
Z0, Z1, ..., Zn	Independent variables
Subscript	
exp	Experimental
comp	Computational
Greek Letters	
λR	Relative error, %
ω	Uncertainty
ρ_∞	fluid density (kg/m³).

References

[1] Baker, N., and Steemers, K. "Energy and Environment in Architecture: A Technical Design Guide", EE & FNSpon, London, 2000.

[2] Oscar, H., Natural Ventilation: Strategies, Health Implications and Impacts on the Environment, NOVA Publication, New York, 2015.

[3] Williams, C., Islamic Monuments in Cairo: The Practical Guide, The American University in Cairo Press, Egypt, 2008.

[4] Wong, N., and Heryanto, S. "The Study of Active Stack Effect To Enhance Natural Ventilation Using Wind Tunnel And Computational Fluid Dynamics (CFD) Simulations." Energy and Buildings, 36 2004, 668-678.

[5] Chu, C., Chiu, Y., Tsai, Y., and Wu, S., "Wind-Driven Natural Ventilation for Buildings with Two Openings on the Same External Wall", Energy and Buildings, 2015, 108, 365-372.

[6] Wang, H., Karava, P., and Chen, Q., "Development of Simple Semiempirical Models for Calculating Airflow through Hopper, Awning, and Casement Windows for Single-Sided Natural Ventilation", Energy and Buildings, 2015, 96, 373-384.

[7] Sacht, H., Bragança, L., Almeida, M., and Caram, R., "Study of Natural Ventilation in Wind Tunnels and Influence of the Position of Ventilation Modules and Types of Grids on a Modular Façade System", Energy Procedia, 2016, 96, 953-964.

[8] Mohandes, S., Zhang, X., and Mahdiyar, A., "A Comprehensive Review on the Application of Artificial Neural Networks in Building Energy Analysis", Neurocomputing, 2019, 340, 55-75.

[9] Consumption of Energy, European Commission, http://ec.europa.eu/ [Last seen May 2020]

[10] Owusu, P., and Asumadu-Sarkodie, S., "A Review of Renewable Energy Sources, Sustainability Issues and Climate Change Mitigation", Cogent Engineering, 2016, 3 (1), 1-14.

[11] D'Amico, A., Ciulla, G., Traverso, M., Lo Brano, V., and Palumbo, E., "Artificial Neural Networks to assess Energy And Environmental Performance Of Buildings: An Italian Case Study", Journal of Cleaner Production, 2019, 239, 117993.

[12] Laia, D., Qib, Y., Liub, J., Daib, X., Zhaob, L., and Weic, S., "Ventilation Behavior in Residential Buildings with Mechanical Ventilation Systems across Different Climate Zones in China", Building and Environment, 2018, 143, 679-690.

[13] Yao, M., and Zhao, B., "Window Opening Behavior of Occupants in Residential Buildings in Beijing", Build. Environ., 2017, 124, 441-449.

[14] Chena, J., Bragerb, G., Augenbroec, G., and Songa, X., "Impact of Outdoor Air Quality on the Natural Ventilation Usage of Commercial, Buildings in the US", Applied Energy, 235, 2019, 673-684.

[15] Demuth H., and Beale, M., Neural Network Toolbox, MathWorks., Inc, 2000.

[16] Zhao, H., Magoulès, F., "A Review on the Prediction of Building Energy Consumption", Renew. Sustain. Energy Rev., 2012, 16, 3586-3592.

[17] Sözen, A., Akçayol, M., and Arcaklio ˘glu, A., "Forecasting Net Energy Consumption Using Artificial Neural Network", Energy Sour, 2006, Part B 1, 147-155.

[18] Yang, J., Rivard, H., and Zmeureanu, R., "Building Energy Prediction with Adaptive Artificial Neural Networks", Proceedings of the Ninth International IBPSA Conference, Montréal, Canada, August, 2005, 15-18.

[19] Dai, X., Liu, J., Zhang, X., and Chen., W., "An Artificial Neural Network Model Using Outdoor Environmental Parameters and Residential Building Characteristics for

Predicting the Night Time Natural Ventilation Effect", Building and Environment ,2019, 159, 106139.
[20] Afroza, Z., Urmeea, T., Shafiullaha, G., and Higginsb, G., "Real-time Prediction Model for Indoor Temperature in a Commercial Building", Applied Energy, 2018, 231, 29-53.
[21] Park, J., and Choi, C., "Modeling Occupant Behavior of the Manual Control of Windows in Residential Buildings", Indoor Air, 2019, 29(2), 242-251.
[22] Mohammed, A. G., Abdel Gawad, A. F., and Nassief, M. M., "Computational and Experimental Investigations of the Impacts of Window Parameters on Indoor Natural Ventilation in "Sultan Al-Ashraf Qaytbay" Mosque", Journal of Advanced Research in Fluid Mechanics and Thermal Sciences, 2020, 69(2), 19-41.
[23] Egyptian Ministry of Antiquities, http://www.antiquities.gov.eg/ [Last seen May 2020]
[24] Cui, C., Cai, W., and Chen, H., "Airflow Measurements Using Averaging Pitot Tube under Restricted Conditions", Building and Environment, 2018, 179, 17-26.
[25] Keramidas, G., and Brebbia, C. "Computational Methods and Experimental Measurements", Proceedings of the International Conference-Washington DC." Springer-Verlag Berlin Heidelberg GmbH, 1982.
[26] James, D. and Freeman, A., Neural Networks Algorithms, Applications, and Programming Techniques, Addison-Wesley, 1991.
[27] Hykin, S., Kalman Filtering and Neural Networks, Ontario, Canada: A Wiley-Interscience., 2001.
[28] James, D., and Freeman, A., Neural Networks Algorithms, Applications, and Programming Techniques, Addison-Wesley, 1991.
[29] Hahnloser, R. Sarpeshkar, R., Mahowald, M., Douglas, R., and Seung, H., "Digital Selection and Analogue Amplification Coexist in a Cortex-Inspired Silicon Circuit", Nature, 2000, 405(6789), 947.
[30] Kasabov, N., Foundations of Neural Networks, Fuzzy Systems, and Knowledge Engineering, London: A Bradford Book, 1998.